PAPER Nr. : 113

RECENT IMPROVEMENTS IN ROTOR TESTING CAPABILITIES IN THE ONERA S1MA WIND TUNNEL

BY

P. CROZIER

ONERA, GRANDS MOYENS D'ESSAIS
MODANE, FRANCE

TWENTIETH EUROPEAN ROTORCRAFT FORUM
OCTOBER 4 - 7, 1994 AMSTERDAM

Printed by the Technical Highschool Haarlem

RECENT IMPROVEMENTS IN ROTOR TESTING CAPABILITIES IN THE ONERA S1MA WIND TUNNEL

by P. Crozier (ONERA / GME)

Abstract

Since 1988, helicopter rotor tests in the large S1MA wind tunnel at the Modane-Avrieux Center of Onera have been conducted with a helicopter rotor rig that improves test productivity and measurement accuracy. With this device, the test methods have considerably evolved . Nowadays, rotor performance comparisons are possible without interpolation. Moreover local measurements on different rotors, such as dynamic pressures or stresses, and acoustic measurements, can be compared directly with iso-performances.

In addition, a scanner device has been developped by ONERA. In use since 1991, it enables tests to be carried out with more than 440 on board measurements.

First this document presents the characteristics of the helicopter rotor rig and the acoustic lining designed to reduce noise reflexions of the walls. Secondly, the description of the rotor used during the eleventh test series, the features of the scanner device and the way tests are now conducted, are shown. Finally, the wall correction effects, the quality of the results for performances and local measurements are presented.

Notations

a : Sound speed, m/s
V0 : Freestream velocity, m/s

ρ : air density, kg/m^3
P0 : Freestream static pressure, Pa
M0 : Freestream Mach number = V/a

b : Number of blades
R : Rotor radius, m

D : Rotor diameter, m

r/R : Relative radius

C : Airfoil chord, m

X/C : Relative chord (leading edge as origin)

σ : Rotor solidity = (b*C)/(Π*R)

Ω : Rotor angular velocity, rad/s

μ : Rotor advance ratio = V/(ΩR)

MωR : Rotational tip Mach number = ΩR/a

α : Rotor shaft tilt angle, degrees

ψ : Rotor blade azimuth angle, degrees

Ψ = 0°when blade 1 at rear
V : Velocity in the rotor plane after wall and support corrections, m/s

$\Delta\alpha$: local angle of attack, degrees

$\Delta\beta$: local yaw, degrees

θ : Blade pitch angle, degrees

θ0 : Blade collective pitch angle, degrees

θ1c : Lateral cyclic pitch, degrees

θ1s : Longitudinal cyclic pitch, degrees

$\theta(\psi) = \theta 0 + \theta 1c*\cos(\psi) + \theta 1s*\sin(\psi)$

β : Blade flapping angle, degrees

β0 : Blade collective flapping angle, degrees

β1c : Longitudinal tilt, degrees

β1s : Lateral tilt, degrees

$\beta(\psi) = \beta 0 + \beta 1c*\cos(\psi) + \beta 1s*\sin(\psi)$
L : Rotor lift, N
T : Rotor propulsion, N
Q : Rotor shaft torque, Nm

CL : Rotor lift coefficient = $L/(\rho*\pi*R^2*(\Omega*R)^2)$
CT:Rotor propulsive coefficient

$CT=T/(\rho*\pi*R^2*(\Omega*R)^2)$
CQ : Rotor torque coefficient

$CQ = Q/(\rho*\pi*R^3*(\Omega*R)^2)$
MN : Local Mach number

$MN = M\omega R*((r/R)+\mu*\sin(\psi))$
P : Pressure mesured by blade sensor
CP : Pressure coefficient

$CP = (P-P0)/(0.7*P0*MN^2)$
CN : Section normal force coefficient (blade section axes)

1) INTRODUCTION :

For more than twenty five years, ONERA has been conducting rotor tests in the S1MA wind tunnel for helicopter manufacturers (Ref 1, 2, 3).

During this period, the test objectives have considerably changed and numerous improvements have taken place in the test facilities.

One of the most complex tests, requested jointly by EUROCOPTER and ONERA Aerodynamics Department was carried out in 1991 on two four-bladed rotors similar to those of a 1/4 scale Super Puma. The first one had a rectangular tip (7A rotor) and the second one a sweep and anhedral tip blade (subsequently refered to in this paper as 7AD1 tip). The purposes of this test were to estimate the effect of the 7AD1 tip and to determine accurately the local airflow on the blades in a large flight envelope. It was therefore necessary to have a good productivity and to accurately measure a great number of pressures. To complete the knowledge of the boundary layer some hot films were fitted on the blades.

This document briefly describes the helicopter rotor rig and the acoustic lining and, in particular, the rotor tested during the eleventh test and the electronic scanning device used to convey the data. In addition, the way tests are conducted, wall and support effect corrections and the quality of the results are also presented.

2) THE TEST RIG :

2.1 Specification :

The rig is designed to be installed in one of the three movable test sections of the large S1MA wind tunnel of the Modane-Avrieux Center (Ref 4). The test section is 8 m in diameter and 14 m in length (Fig 1). For helicopter rotor tests the maximum airspeed is 130 m/s but this wind tunnel can reach Mach number 1.

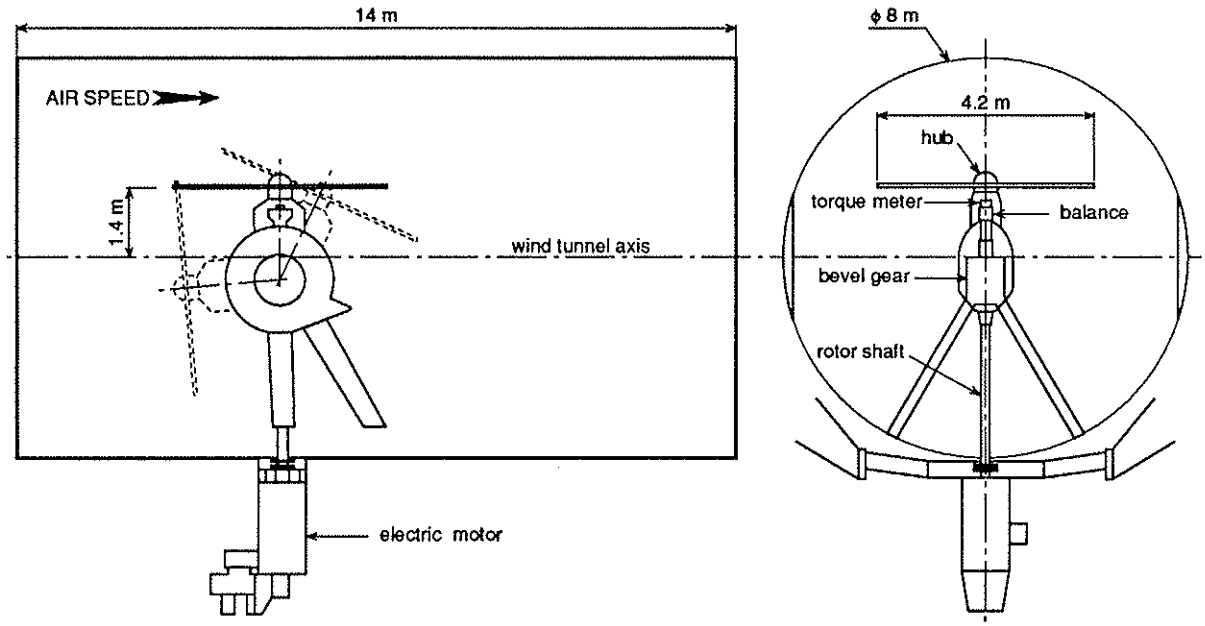

Figure 1 : rotor test rig in S1MA

In order to test a 4.2 m rotor the features of the rig are :

- rotation in clockwise or counter clockwise direction
- rotation speed between 0 and 1100 rpm
- maximum power 500 kW
- maximum torque 7000 Nm at 680 rpm
- tilt angle range +20° to -95° with a positionning accuracy of ± 0.02 degrees

- accurate rotation speed control for rig and model safety :

- the rotor must never be stopped in the presence of wind in the test section

- fast variations in rotation speed are forbidden

To ensure the stability of the rotation speed a sophisticated regulation is used. During a parameter variation, the stability is ensured within ± 2% and within ± 0.2% during measurement phases.

- first longitudinal eigenmode higher than the rotation frequency to avoid any risk of ground resonance

- only four days of installation before entry into the wind tunnel itself, so as to increase test productivity

2.2) Description :

The test rig includes three main parts : the drive system, the structure supporting the rotor and the measuring instruments.

2.2.1) Drive system

The electric drive motor is installed vertically under the test section. To ensure perfect speed control, several systems are also fitted with the motor in the basement of the wind tunnel. Among these one can mention the DC generator and backup systems in case of a line power failure (Fig 2).

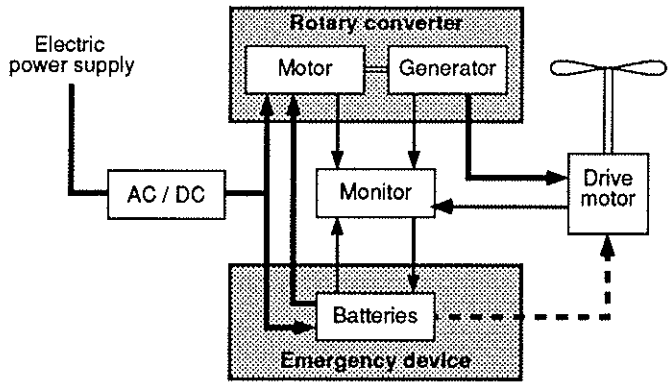

Figure 2 : drive system block diagram

A checking system is provided to protect the installation against the different possibilities of power failure :

- short power cut, by the inertia of the DC generator

- power cut, by batteries for two minutes

- direct switchover to the batteries in case of a failure detected on the converter unit.

2.2.2) Supporting structure

The structure, called bevel gear, supports the rotor, but also tilts and drives the shaft in rotation. It includes a fixed part and a tilting part. The tilting center is located near the center line of the test section and tilting is achieved by a motor-driven wormscrew-gear assembly. Another wormscrew-gear assembly ensures locking in position.The maximum tilting rate is two degrees per second.

2.2.3) Measuring instruments

The measuring instruments (balance, torquemeter and flectors) are an integral part of the test rig, since they provide the mechanical connection between the tilting part of the bevel gear and the rotor.

2.2.3.1) Balance

The balance is non-rotating with assembled plates, connected by six dynamometers. The lower plate is attached to the tilting part of the bevel gear and the upper plate supports the rotor.

The dynamometers are interchangeable. Three dynamometers measure the lift, roll, and pitch moments, two measure the lateral force and rotor bearing friction moment and one measures the propulsive force. All the dynamometers have a capacity of 20 000 N.

These dynamometers are apparently oversized because, during such tests, dynamic excitation added to static load could overload the balance.

The balance is also equipped with a safety device which can lock the upper plate. Three remote control locks are released if one of the dynamometers exceeds a preset load.

2.2.3.2) The torquemeter and flectors

The torquemeter is a thin tube used to measure the motor torque supplied to the rotor. It is located on the transmission line inside the balance and has a capacity of 3 000 Nm.

The flectors, which are a decoupling device, are located on both sides of the torquemeter. They transmit the motor torque but are very flexible in other planes so as not to short-circuit the balance. Their residual stiffness is taken into account thanks to a strain gauge located on the upper flector.

With the helicopter test rig an accuracy in rotor performance measurements of approximately ± 1% is obtained.

3) THE ACOUSTIC LINING :

The S1MA wind tunnel is particularly well suited for impulsive noise studies for high advance ratio configurations. Therefore, during helicopter tests, acoustic measurements are always done. The typical experimental set-up is shown in figure 3.

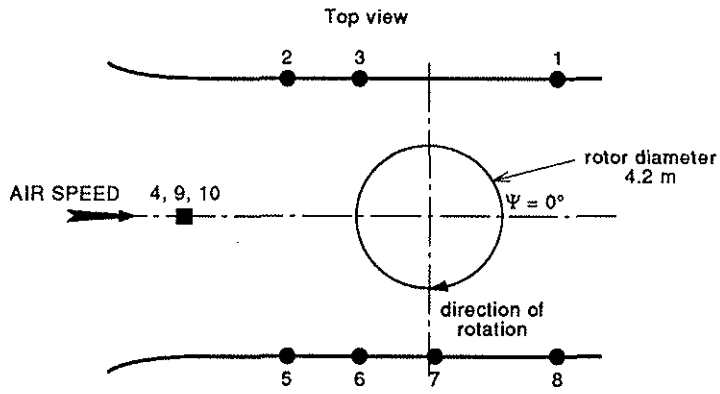

Figure 3 : positioning ofmicrophones in S1MA

Seven microphones (1, 2, 3, 5, 6, 7, 8) are fixed on the wind tunnel walls in the rotor plane and three (4, 9, 10) are on a mast in front of the rotor. Microphones 2, 5, 4, 9 and 10 are in the far field (≥ 1.5 D). Measurements only concern harmonic rotor noise due to the periodic phenomena caused by blade rotation. Therefore, a synchronous rotation analysis enables the suppression of broadband noise and other harmonic noise not generated by the rotor. 1024 points are acquired per rotor revolution (about 16 kHz).

To decrease wall reflections acoustic lining can be used. It has no effect on rotor performance but is particularly efficient acoustically for high advance ratio. Figure 4 shows the comparison with and without the acoustic lining for an advance ratio μ=0.5. All the microphones presented show a noise decrease between 3 and 8 dB.

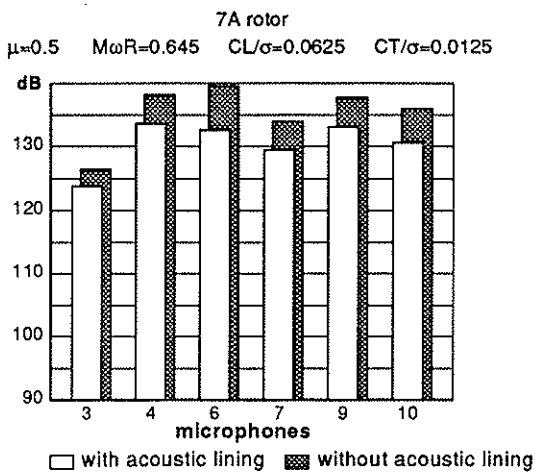

Figure 4 : acoustic lining effect

For acoustic rotor comparisons the more interesting microphones are those located on the mast. In fact, they measure the high speed noise which is maximum in the advancing direction. Figure 5 shows the acoustic pressures measured by microphone n°4 with 7A and 7AD1 rotors (7AD1 tips). The advance ratio is μ=0.4, the lift coefficient CL/σ=0.075 and the rotational tip Mach number MωR=0.645.

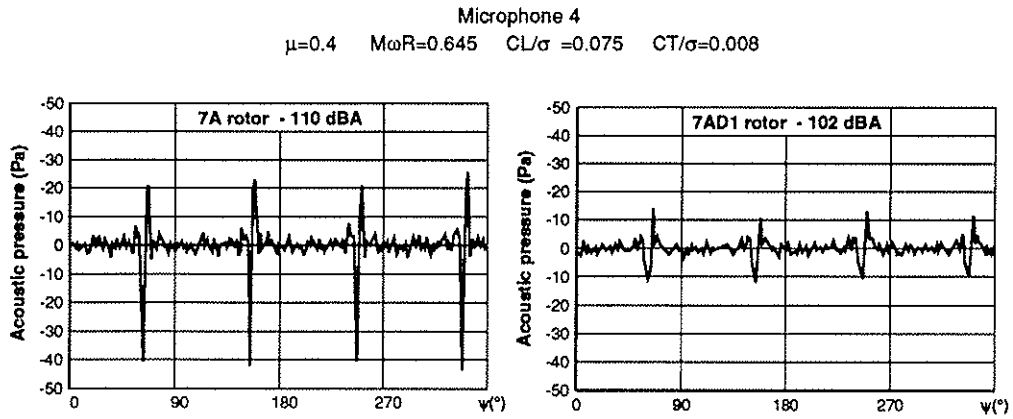

Figure 5 : 7A-7AD1 acoustic comparison

With the 7AD1 tip an improvement of 8 dB is obtained (Ref 5).

4) ROTOR DESCRIPTION :

During the eleventh test series at S1MA, in addition to the standard measurements (balance, torquemeter, pitch, flapping...), a large number of pressure sensors and hot films were installed to determine precisely the local airflow on the blades.

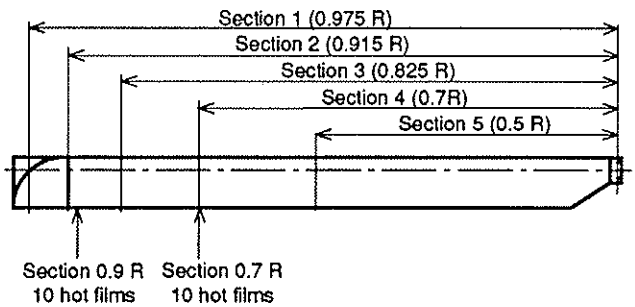

Figure 6 : blade transducer locations

Five sections (sections 1, 2, 3, 4, 5) are instrumented with pressure transducers and twenty hot films are distributed over two stations.As the twenty pressure sensors of one section cannot be installed on only one blade they are distributed over three blades.

Temperature compensation is insufficient to ensure the accuracy of pressure measurements. Pressures have therefore to be corrected for temperature effects.

The hot film specification was set to ensure :

- good sensitivity (warmed surface has to be as small as possible)

- easy implementation without changing the airfoil geometry (thickness : 0.3 μm)

The measurement principle lies in keeping the temperature of the sensitive element constant. The power needed to maintain a constant temperature depends on the heat transfer and thus of the boundary layer state.

Hot film electronics are on board, because in order to work properly the distance between the bridge and its electronics has to be less than 5 m.

All the sensors measured during the eleventh test series are presented below :

Designation	Number	Accuracy
Torquemeter	1	0.1%
Flector	1	1 N
Pitch, flapping and lead-lag of two blades	6	± 0.02°
Absolute pressure sensors	118	0.2%
Temperature of each pressure sensor	118	0.3°
Strain gauges	58	1%
Hot films	20	
Hub gauges	5	1%
Hub accelerometers	3	3%
Total	330	

The rotational speed range is 12 to 17 revolutions per second. A magnetic sensor, fitted in front of a 128 cog-wheel, works as an external clock for data acquisition.

To ensure model safety some measurements are not scanned (torquemeter, flector, flapping, pitch, some strain gauges...). They pass straight through the slip ring.

The scanned measurements :

- pressure sensors : it is considered that sensor temperature is stable for one measuring point. Recording is done just before the acquisition of the corresponding pressure signal (low-pass filters set at 0.5 Hz).Pressure signals are acquired 128 times per revolution during 30 successive turns. A very good simultaneity for data acquisition is required, so the implementation of "sample and hold" is necessary.

- hot films : like the pressure sensor data is acquired 128 times per revolution during 30 successive turns (filtered 1000Hz).

- strain gauges : for this kind of sensors 64 acquisitions are done per revolution during 10 turns.

5) THE SCANNER DEVICE :

For such a test (330 measurements), a scanner device was necessary to convey the data, because neither the slip ring located inside the transmission shaft, nor the S1MA acquisition system, were able to acquire simultaneously all the measurements. As a reminder the slip ring has 137 measurement tracks (about 67 measurements) and 13 power tracks while the S1MA acquisition system has 80 analog channels.

5.1) Electronic part :

Different solutions were studied by ONERA, and, in the end, an analog electronic device was chosen for its accuracy, its reusability, its small volume and its reliability even under vibration.

The basic element of the electronic scanner device is an eight channel switch also called multiplexer. Figure 7 shows the block diagram of this device.

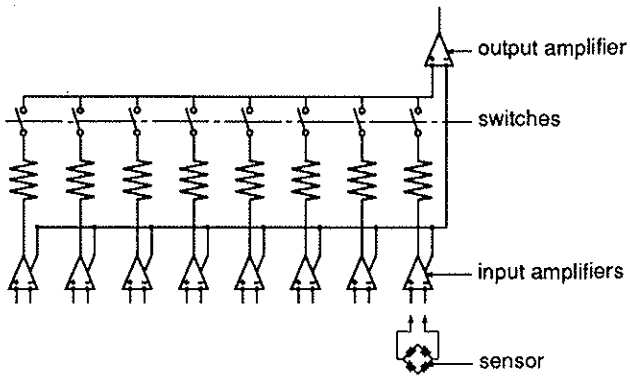

Figure 7 : multiplexer block diagram

The eight inputs pass through eight amplifiers, after which one of the eight inputs is selected and sent towards the output amplifier.

- The input amplifier :

Differential amplifiers are used for their accuracy. They have a very high input impedance, a very low sensitivity to temperature and their gains can be chosen between 1 and 1000 with external resistors.

- The scanner :

This is an analogic multiplexer, using CMOS technology. It is connected to the differential amplifiers through protective resistors. Three opto-coupling devices chosen for their low input current prevent interference between the multiplexer adressing and measurement.

- The output amplifier :

The purpose of this amplifier is to provide an output impedance consistent with the impedance of a one hundred meter length cable (like those used between the test section and the S1MA acquisition system).

The main electronic characteristics are :

- dissipated power 720 mW per multiplexer
- stabilized temperature 40°C (with an ambient temperature of 20°C)
- good linearity
- zero drift lower than 0.3 mV after fourteen hours of work
- band width higher than 50 kHz
- background noise lower than 10 mV with 100 meters of cable in output

All these qualities make it the basic element of the electronic scanner device.

5.2) Mechanical description :

During the eleventh test series two rings each of 20 multiplexers enabled data acquisition of twenty pressure sensors and their twenty temperatures, while a third ring of fifteen multiplexers was used for acquisition of the strain gauges and the hot films. The whole capacity of the scanner device was therefore 440 measurements (55*8).

Today, up to five rings can be used : three of twenty multiplexers and two of fifteen multiplexers, thus increasing the measurement capacity up to 720 channels.

To keep low the working temperature of the scanner, the heat has to be drained off. For this the structure supporting the ring is made of brass and some brass parts are put between each multiplexer and the brass structure.

5.3) Positioning of the scanner system :

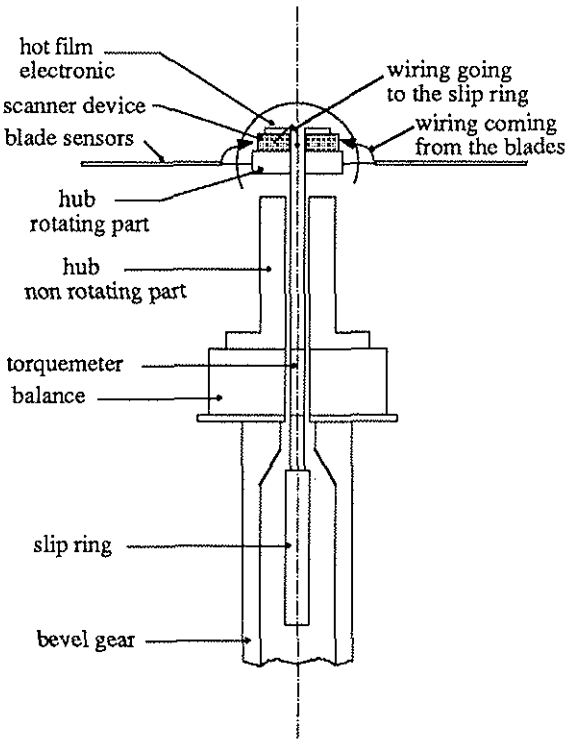

Figure 8 : positioning of the scanner system

The scanner device is located in the upper part of the hub. The volume needed to fit the scanner device is 3000 cm^3.

5.4) Functioning of the scanner :

5.4.1) Adjustment

To avoid electrical interference when all the blade sensors are connected (55 multiplexers), filters are placed on the inputs and outputs of the multiplexers. Since it cannot be done in the multiplexers, the resistors and capacitances are fixed on the copper connexions of the printed circuit holding the multiplexers. The transfer function obtained is presented in figure 9.

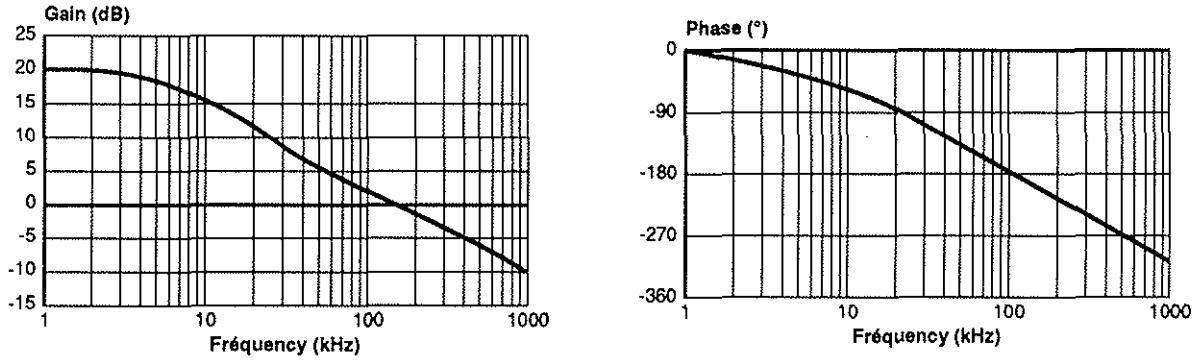

Figure 9 : multiplexer transfer function

The band width is 0-3 kHz which is fully consistent with present data acquisition requirements.

5.4.2) Calibration

To determine the calibration for each channel of measurement a known voltage is applied at each input and the output voltage is measured. The input voltage is provided by a voltage generator of ± 10V within ± 1 mV.

Before the calibration, linearity, stability with temperature, and stability in time are noted.

5.4.2.1) Linearity

Ve : input voltage; Vs : output voltage

Vs = A0 + A1* Ve A0 : zero lag A1 : gain

Measurements are done volt per volt between -9 and +9 volts.

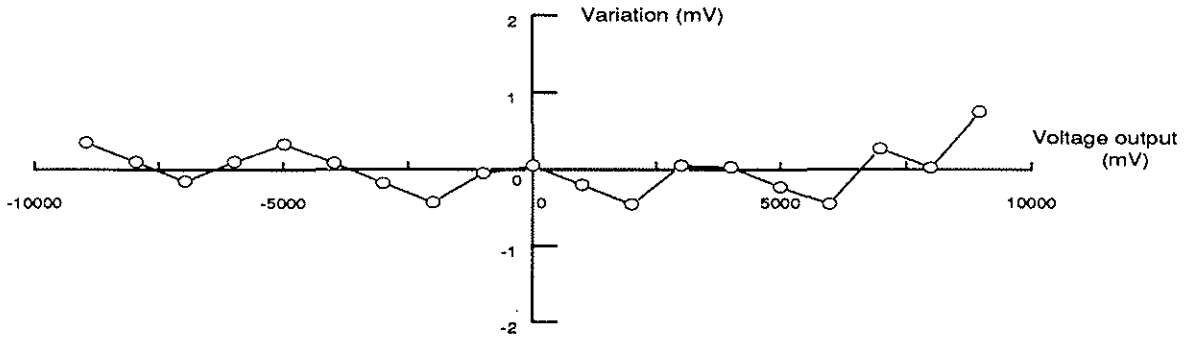

Figure 10 : deviation between the linear law and the measurements

The deviation between the linear law and the measurements is lower than 1 mV for the whole width of the band. This linearity is very good.

5.4.2.2) Stability in time

Two calibrations were done, the first one in March 1990 and the second one in March 1991.

DA0 = A0(second calibration) - A0(first calibration)

DA1/A1 = (A1(second calibration) - A1(first calibration)) / A1(first calibration)

The following figure (Fig 11) presents the results for all the even numbered multiplexers of ring number one for the first level of commutation.

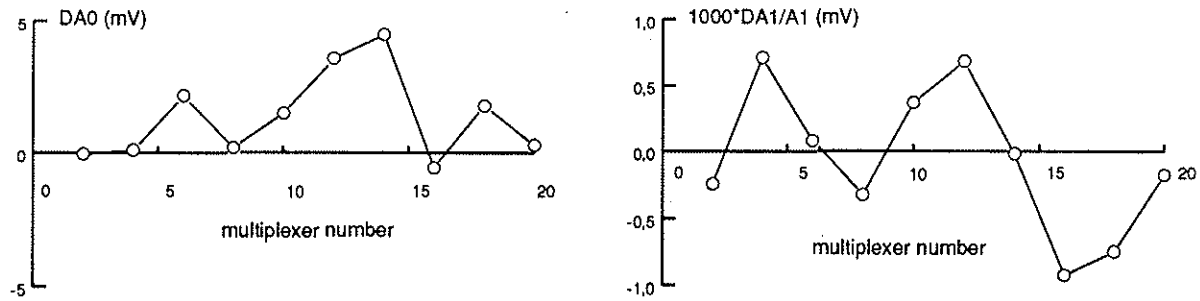

Figure 11 : multiplexer stability in time

The differences DA0 are lower than 5 mV and DA1/A1 does not exceed 1/1000. For all the multiplexers the results are as good as those presented. The stability in time is satisfactory.

5.4.2.3) Stability with temperature

Some calibrations were done at 40°C and 60°C

DA0 = A0(60°C) - A0(40°C)

DA1 = A1(60°C) - A1(40°C)

Figure 12 shows the results for all the multiplexers of ring number one for the first level of commutation.

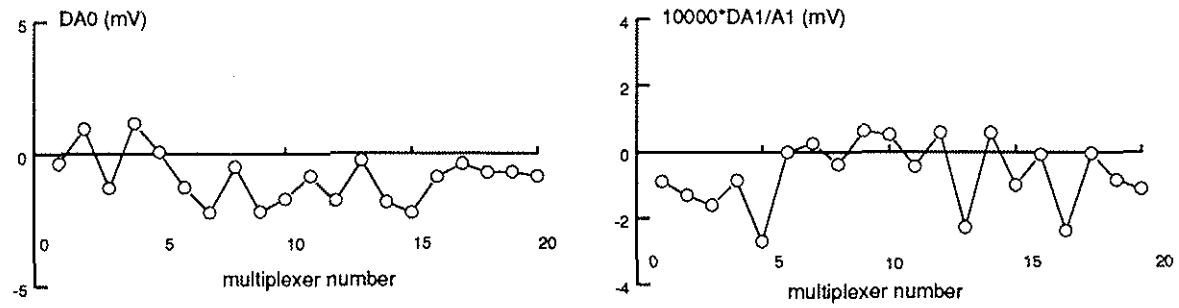

Figure 12 : multiplexer stability with temperature

The differences for the constants A0 are lower than 2.5 mV and for the slope the variations are lower than $3*10^{-4}$. The stability with temperature is satisfying.

5.5) Scanner device use :

The scanner device was used for the first time in a wind tunnel helicopter test during the eleventh test series at S1MA in May-June 1991.

In test, as soon as measurement conditions are respected (advance ratio Mu, rotational tip Mach number MωR, lift, thrust and cyclic control law) an automatic sequence enables the measurements for each scanner position to be recorded.

The data which cross the slip ring are filtered by low-pass filter amplifiers set at 1000 Hz - 12 dB/octave.

For one measuring point 900 000 data were acquired. 180 measuring points were done during the test.

6) TEST METHODOLOGY :

Before 1987 a measurement point consisted of a sweep of the rotor collective pitch at a given rotor tilt angle (Ref 6). This method had two major drawbacks :

- interpolating and smoothing of the performance curves was necessary in order to perform rotor performance comparisons at equal lift and propulsion;

- comparing the vibratory and acoustic behaviour of rotors was difficult.

To avoid these problems it was decided to use another rotor control method. The torque moment provided at the blades is measured when the following six "piloting conditions" are reached :

- advance ratio, μ

- rotational tip Mach number, MωR

-lift coefficient, CL/σ

-propulsive coefficient, CT/σ

- cyclic control law : $\beta 1c$, $\beta 1s$.

Two cyclic control laws are used :

- the no-flapping law : $\beta 1c = \beta 1s = 0°$.

- the "Modane" law : $\theta 1s = \beta 1c$ and $\beta 1s = 0$.

This latter is far from piloting reality but it decreases the vibrations.

To respect those six conditions we set :

-the Mach number of the airflow, M0

- the rotor rotational speed, Ω

-the rotor shaft tilt angle, α

-the collective pitch, $\theta 0$

-and the cyclic pitch $\theta 1s$, $\theta 1c$

To improve productivity, on line software to assist rotor piloting has been set up.

This method enables the comparison of rotor performances, local measurements and dynamic behaviour in real time. It becomes therefore possible to select, during a test campaign, the rotor for which the maximum amount of data should be acquired.

For the performance measurements the hub effect must be taken into account. The tests begin by blade-off test for several advance ratio, rotor shaft tilt angle and collective pitches. The global load measurements are then corrected for hub effects to obtain the performance of the blades in real time.

7) WALL AND SUPPORT INTERFERENCE CORRECTIONS :

To compare performance measurements with performance calculations in an infinite atmosphere, wall and support effects are taken into account (Ref 7).

With the description of the rotor wake in an infinite atmosphere given by the ONERA Aerodynamics Department, the Large Testing Facilities Department calculates wall and support disturbance in the rotor plane for each Mach number and tilt angle of the rotor. 2436 panels are used to modelize the wind tunnel walls and 2150 panels for the test rig. Disturbance results are given from $\Psi = 0°$ to 360° every 15° and between r/R = 0.3 and 1 every 0.1; thus 475 points. Three quantities are used to qualify the speed disturbances : the ratio between the corrected velocity and the freestream velocity (V/V0), the longitudinal and lateral angles between V and V0 ($\Delta\alpha$ and $\Delta\beta$). Some disturbance results for M0 = 0.29 and $\alpha = -16°$ are presented in figures 13a, 13b and 13c.

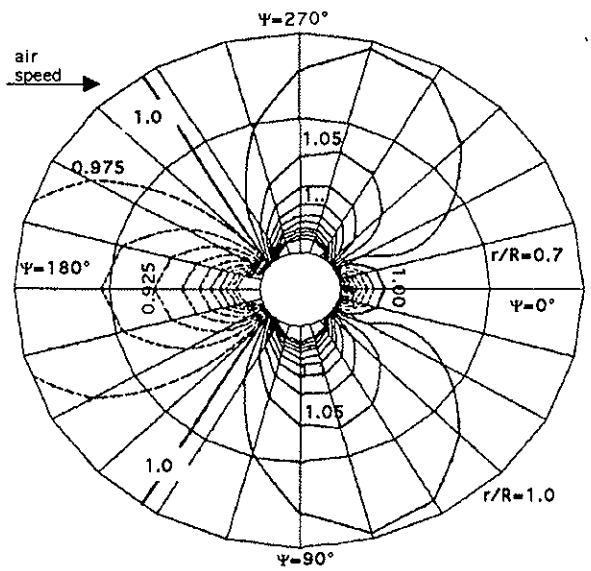

Figure 13a : V/V0

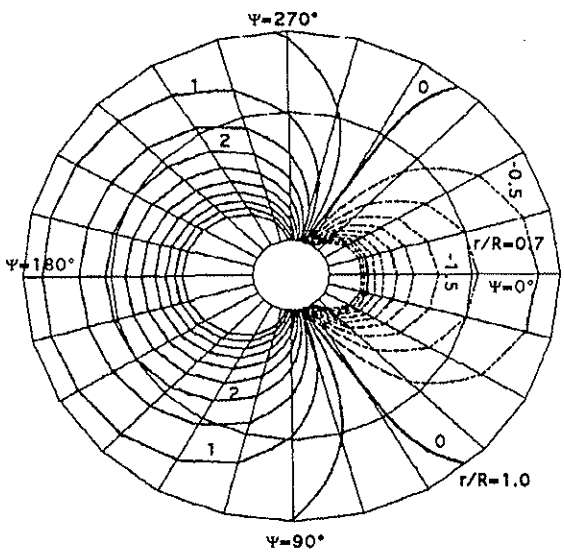

Figure 13b : $\Delta\alpha$

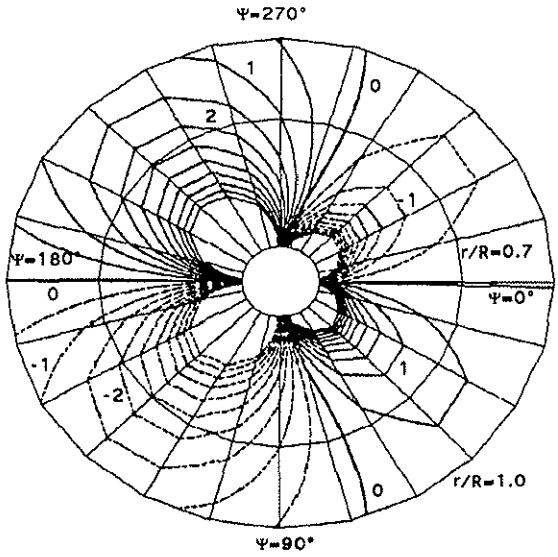

Figure 13c : $\Delta\beta$

One can see a very good symmetry between the advancing and the retreating blade for the V/V0 and $\Delta\alpha$ distributions when $\Delta\beta$ distribution is nearly asymmetrical. Therefore to reduce time calculation the speed disturbances are computed only for the advancing blade.

Then the speed disturbances are introduced into the rotor performance calculations. The wake effects can also be considered. Figure 14 presents the correction effects for torque coefficient.

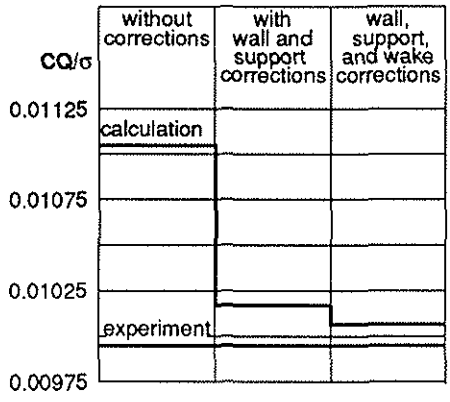

Figure 14 : correction effects for torque coefficient

The comparison between calculation and experiment clearly improves when disturbance in the rotor plane is considered. 90% of the variation in torque coefficient between calculations in an infinite atmosphere and experiment can be explained by wall and support effects. The wake effect contributes by less than 10% in the wall and support interference corrections.

8) MEASUREMENT QUALITY :

The results shown in this section illustrate not only the quality of the rotor performance measurements but also the diversity, quality and amount of local measurements obtained with the on board scanner device.

8.1) Repeatability of performance measurements :

During the tests, repeatability tests are conducted to check the stability of the instrumentation and the ability to establish and maintain consistent test conditions. Figure 15 presents the repeatability of the tests during the eleventh test series. The curve of lift versus torque is supplied within test limits with an accuracy of around 1%, which is the stated goal.

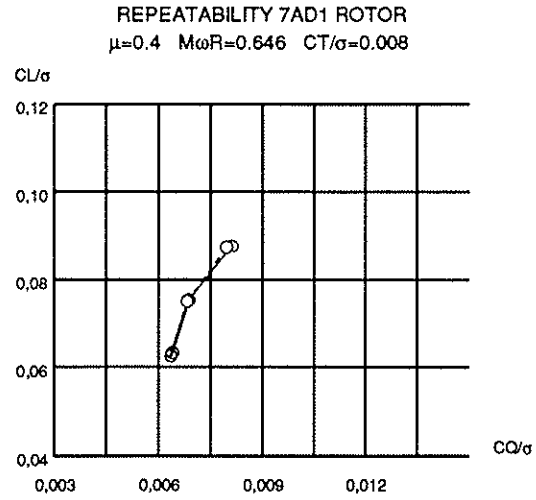

Figure 15 : rotor performance repeatability

8.2) Comparison of rotor performance :

Figure 16 shows, with the same scale as figure 15, the comparative performance of the basic 7A rotor and the 7AD1 rotor. The comparisons are established for advance ratio μ=0.3, 0.4, 0.45 and 0.5 and a rotational tip Mach number MωR=0.646.

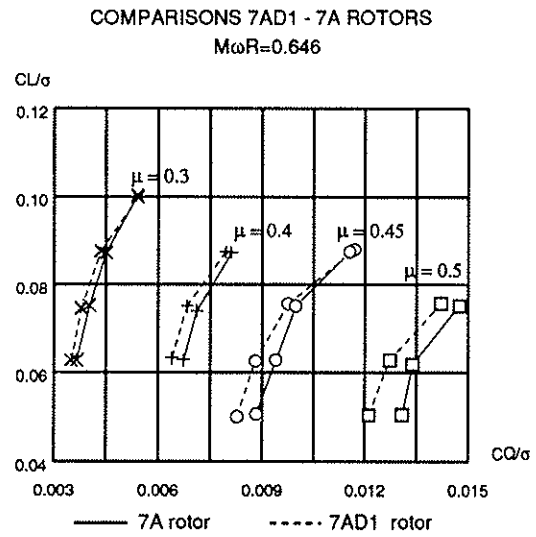

Figure 16 : rotor performance comparisons

7AD1 rotor still gives better performance. Such curves are plotted in real time during the test series.

8.3) Local measurements :

Local measurements are taken via pressure, hot film and stress sensors fitted on the rotor blades. In this section only pressure and hot film results are presented.

8.3.1) pressure

Figure 17 shows the pressure coefficient CP versus azimuthal location Ψ for both tips. The sensors presented are located near the leading edge (X/C = 2%) at r/R = 0.975 (section 1). With the twenty pressure sensors of section 1 the pressure data can also be presented as chordwise distributions at specific azimuths. Such a plotting is shown in figure 18 for an azimuthal position of 90°.

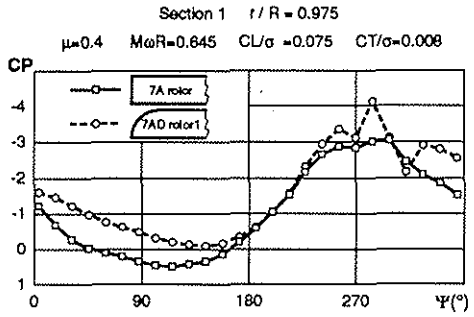

Figure 17 : pressure coefficient against azimuthal location

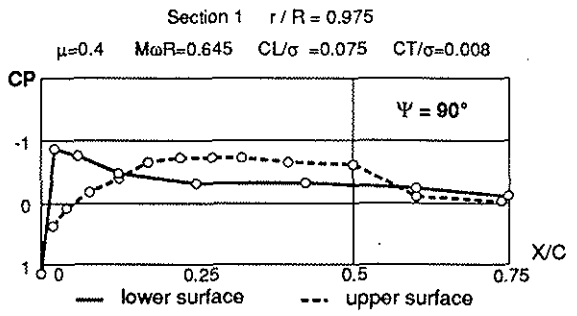

Figure 18 : pressure coefficients versus relative chord

Figure 18, the chordwise distribution is smooth. This observation is significant, since the transducers are distributed on three blades. So the blades are dynamically similar and experience the same flow environment.

Integration of the pressure coefficient distribution results in the local lift coefficient CN (figure19).

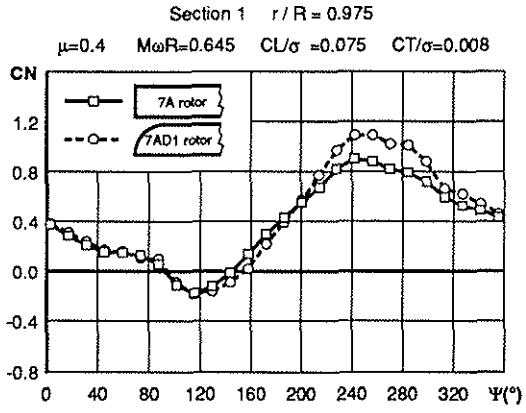

Figure 19 : local lift coefficient against azimuthal position

One can see that the 7AD1 tip is more efficient that the rectangular one.

As for performance measurements good repeatability is observed for the lift coefficient CN. Figure 20 shows three rotor lift coefficients CN versus the blade azimuthal position.

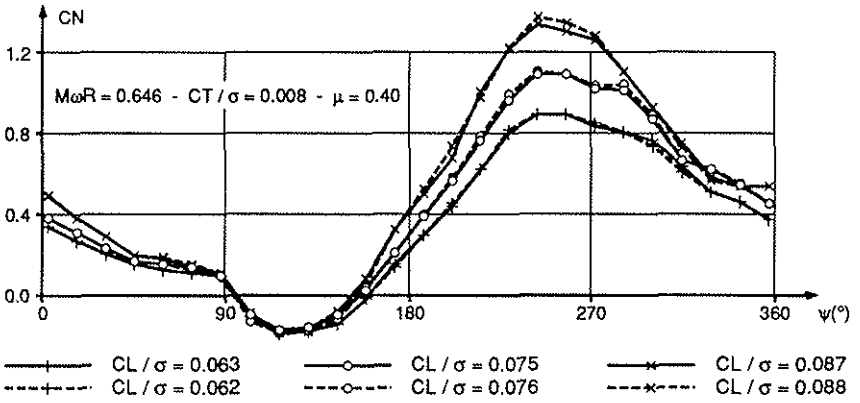

Figure 20 : local measurement repeatability

Such data allows large comparisons with theorical results and the improvement of numerical methods developed by ONERA Aerodynamics Department.

8.3.2) hot films

Two quantities are used to present the hot film results : the mean value of supplied power and its standard deviation. Only the qualitative aspects of the signals are used to determine the boundary layer states. During the rotor revolution, a rapid increase in the mean value reflects

an abrupt increase in the convection coefficient during the boundary layer transition from laminar to turbulent. On the other hand a large standard deviation without corresponding large variations in the mean value indicates a likely flow separation.

The results for hot films located at r/R= 0.9 on the 7A rotor are shown below (Fig 21). The aerodynamic conditions are μ =0.45, MωR = 0.646, CL/σ = 0.075, CT/σ = 0.0101

The first three hot films are mounted on the lower surface, the others are upper surface sensors.

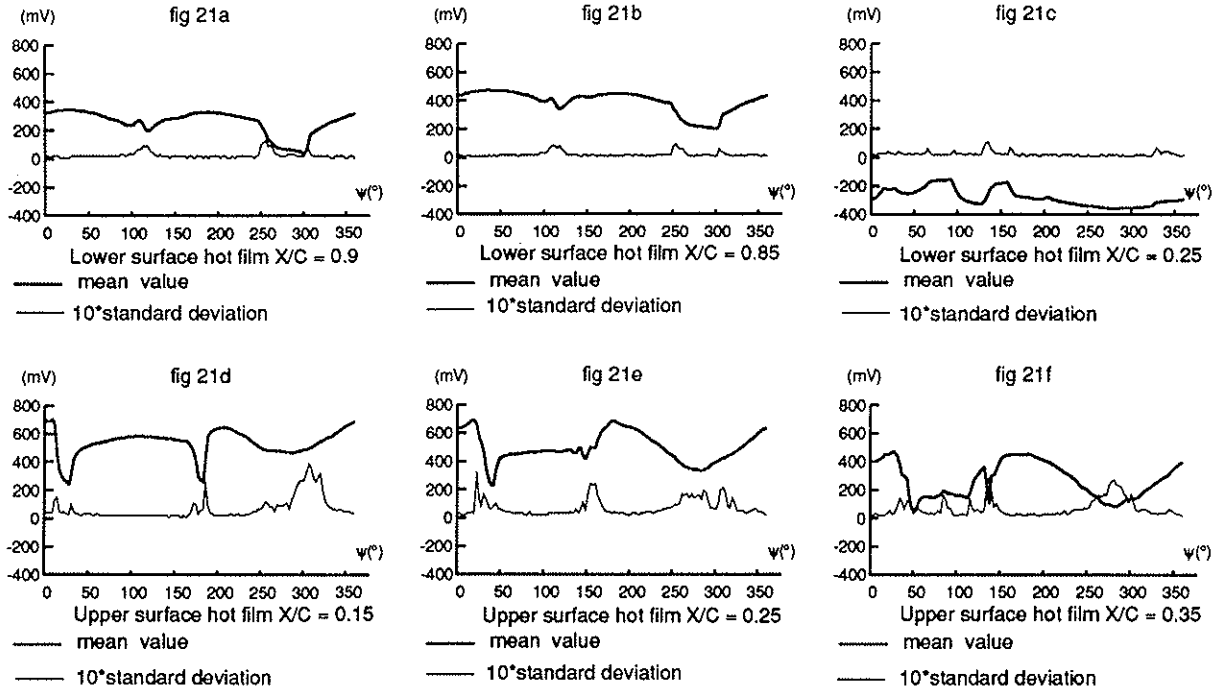

Figure 21 : hot film results

The correlation of the hot film results with the local Mach number distributions in section 2 (r/R = 0.915) enables a better understanding of the source of the phenomena. The local Mach number is computed using the steady, one-dimensional isentropic relation.

$$Ml^2 = \frac{2}{\gamma - 1}\left\{\left[1 + \frac{\gamma}{2} CP\, Mr^2\right]^{\frac{1-\gamma}{\gamma}}\left[1 + \frac{\gamma - 1}{2} Mr^2\right] - 1\right\}$$

Local Mach number distributions in section 2 for different azimuthal positions are presented below (Fig 22) :

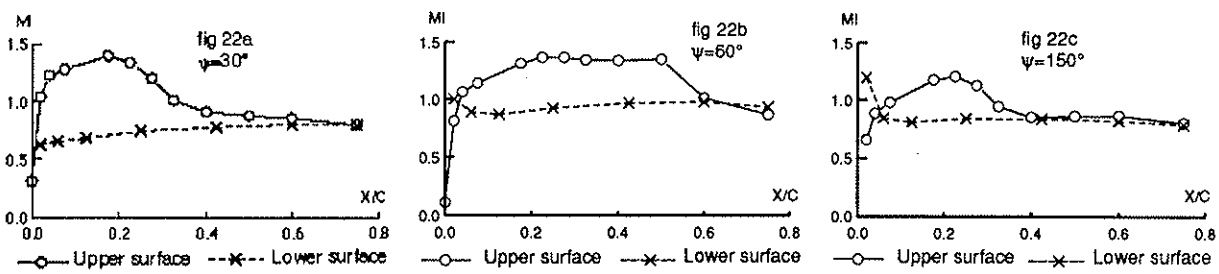

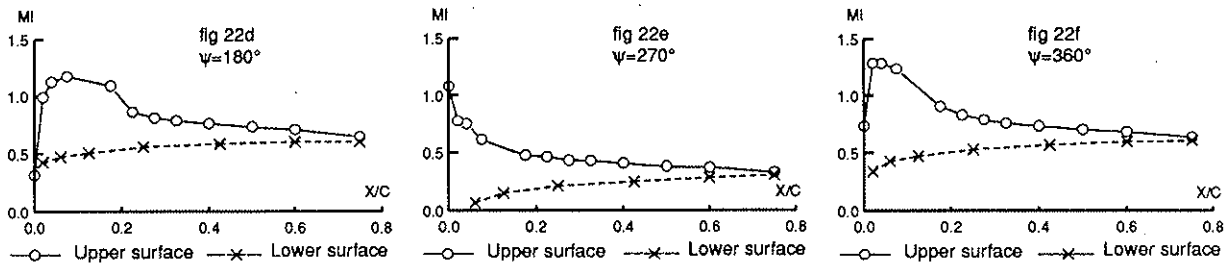

Figure 22 : local Mach number distributions

On the lower surface, for the two relative chords of 0.9 and 0.85, hollows in the mean value in the retreating blade part between 250° and 325°, indicate a short period of laminar flow. Closer to the leading edge (X/C = 0.25) the laminar part is spread out but a small turbulent part still exists between 60° and 160°. With the local Mach number distribution one can see that turbulent boundary layer condition at X/C = 0.25 seems to be closely linked with the leading edge shock that occurs between 60° and 160°. For the other azimuthal positions the lower surface airflow velocity gradient is sufficient to maintain the laminar boundary layer until at least X/C = 0.25.

On the upper surface, near the leading edge (X/C = 0.15) there is a laminar zone between 25° and 175° due to the strong airspeed acceleration between the leading edge and this point (see Ml at $\psi = 30°$, 60°, 150 and 180°). After 180° this point (X/C = 0.15) is located in a decreasing airspeed zone and the boundary layer becomes turbulent. When the distance from the leading edge increases the laminar zone decreases because part of the blade after X/C = 0.3 is very often located behind the shock responsible for laminar-turbulent transition for the advancing blade.

The standard deviation shows upper surface flow separation from X/C = 0.15 between 250° and 325°, and likely lower surface flow separation from X/C = 0.85 between 100° and 125°.

With all these observations the boundary layer state at r/R = 0.9 for different azimuthal positions can be shown (Fig 23). The main hypotheses are :

- if for a given azimuthal position the boundary layer is turbulent at one point, this turbulence continues to the trailing edge.

- the boundary layer is laminar before the upper surface shock and turbulent afterwards.

μ =0.45, MωR = 0.646, CL/σ = 0.075, CT/σ = 0.0101

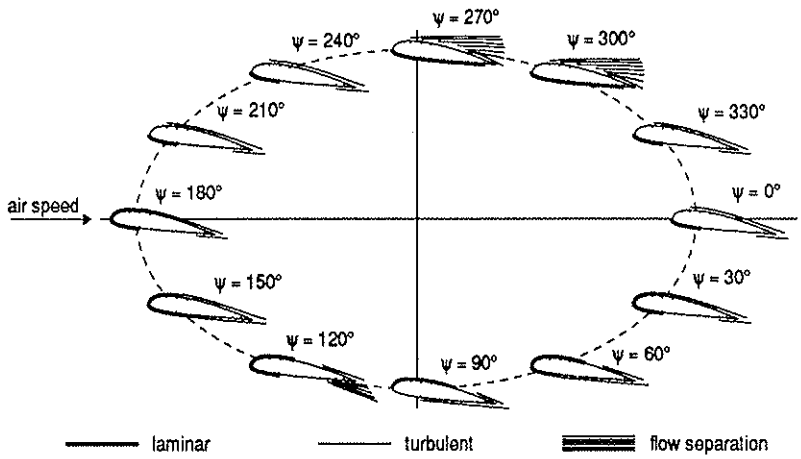

Figure 23 : boundary layer at r/R = 0.9

9) CONCLUSION :

The helicopter test rig used for seven years in the ONERA S1MA large wind tunnel in Modane-Avrieux Center can drive rotors up to 4.2 m in diameter. With this rig, realistic flight conditions have been simulated at very high speed.

The acoustic treatment of the wind tunnel improves the noise measurements particularly for high advance ratio configurations.

In addition, an electronic scanning device, attached to the hub, enables highly instrumented rotors to be tested.

These three devices together with new test methods and the wall and support corrections have enabled a huge data base to be accumulated for each helicopter test and this with good productivity. A large number of these results (performance, dynamic...) are available in real time so the rotor for which the maximum amount of data should be acquired can be selected during the tests.

Later calculations of the acoustics or to determine the boundary layer state are performed to increase the knowledge of that phenomenom and to improve calculation predictions.

Further helicopter tests involving the test rig, the acoustic lining and the scanner device are planned in 1995-1996.

References

Ref 1 : A. Bremond, et al., Design and Wind Tunnel Testing of 1.5 m Diameter Model Rotors.

Paper presented at 4 th European Rotorcraft Forum, September 1976

Ref 2 : J.P. Silvani, et al., Aérospatiale Survey of Wind Tunnel Testing of Small and Large Scale Rotors.

Paper presented at 7 th European Rotorcraft Forum, September 1981

Ref 3 : G. Leclère, et al., Moyens d'Essais d'Hélices et de Rotors de l'ONERA.

Paper presented at 19ème Colloque d'Aérodynamique Appliquée de l'AAAF, Novembre 1982

Ref 4 : M. Allongue, et al., New Rotor Test Rig in the Large Modane Wind Tunnel.

Paper presented at 15 th European Rotorcraft Forum, September 1989

Ref 5 : C. Polacsek, et al., High Speed Impulsive Noise and Aerodynamic Results for Rectangular and Swept Rotor Blade Tip Tests in S1-Modane Wind Tunnel.

Paper presented at 17 th European Rotorcraft Forum, September 1991

Ref 6 : J.P. Drevet, et al., Essais Comparés de Rotor d'Hélicoptère en Soufflerie.

Paper presented at 19ème Colloque d'Aérodynamique Appliquée de l'AAAF, Novembre 1982

Ref 7 : P. Beaumier, et al., Comparisons between FP3D Full Potential Calculations and S1-Modane Wind Tunnel Test Results on Advanced Fully Instrumented Rotors.

Paper presented at 19 th European Rotorcraft Forum, September 1993